Structure
Article

Structure and T Cell Inhibition Properties of B7 Family Member, B7-H3

Vladimir Vigdorovich,[1,*] Udupi A. Ramagopal,[2] Eszter Lázár-Molnár,[1] Eliezer Sylvestre,[1] Jun Sik Lee,[1,5] Kimberly A. Hofmeyer,[1] Xingxing Zang,[1] Stanley G. Nathenson,[1,3] and Steven C. Almo[2,4,*]
[1]Department of Microbiology and Immunology
[2]Department of Biochemistry
[3]Department of Cell Biology
[4]Department of Physiology and Biophysics
Albert Einstein College of Medicine, Bronx, NY 10461, USA
[5]Present address: Department of Biology, College of Natural Science, Chosun University, Gwangju 501-757, Korea
*Correspondence: vladimir.vigdorovich@gmail.com (V.V.), steve.almo@einstein.yu.edu (S.C.A.)
http://dx.doi.org/10.1016/j.str.2013.03.003

SUMMARY

T cell activity is controlled by a combination of antigen-dependent signaling through the T cell receptor and a set of auxiliary signals delivered through antigen-independent interactions, including the recognition of the B7 family of ligands. B7-H3 is a recently identified B7 family member that is strongly overexpressed in a range of cancers and correlates with poor prognosis. We report the crystal structure of murine B7-H3 at a 3 Å resolution, which provides a model for the organization of the IgV and IgC domains within the ectodomain. We demonstrate that B7-H3 inhibits T cell proliferation and show that the FG loop of the IgV domain plays a critical role in this function. B7-H3 crystallized as an unusual dimer arising from the exchange of the G strands in the IgV domains of partner molecules. This arrangement, in combination with previous reports, highlights the dynamic nature and plasticity of the immunoglobulin fold.

INTRODUCTION

T cell activity is controlled by the integration of signals arising from multiple molecular interactions on the cell surface. According to the canonical two-signal model, engagement between the T cell receptor (TCR) and the antigenic peptide:major histocompatibility complex (pMHC) displayed on the surface of the antigen-presenting cell (APC) (i.e., "signal 1") is essential but not sufficient for activation of naive T cells in vivo. This antigen-dependent signal requires additional antigen-independent signals, which can either lead to activation of T cells (e.g., through formation of CD28:B7 complexes) or to downregulation of their activity (e.g., through the formation of CTLA-4:B7 complexes).

The identification of the crucial costimulatory signal through the CD28 receptor was prompted by the observation that in the absence of B7-1 or B7-2 on the APC, engagement of the TCR on naive T cells causes them to become nonresponsive (i.e., anergic) (Sharpe and Freeman, 2002). Once activated, T cells express the inhibitory CTLA-4 receptor, which also binds (and, thus, competes with CD28 for) the B7-1 and B7-2 ligands, providing a control mechanism for T cell proliferation (Sharpe and Freeman, 2002). Additional sequence-related molecules have since been identified and characterized as leading to stimulation (e.g., ICOSL) or inhibition (e.g., PD-L1, PD-L2) of T cell activity via engagement of their corresponding receptors (ICOS and PD-1, respectively), thereby defining the B7 family of proteins (Sharpe and Freeman, 2002). B7 family members belong to the immunoglobulin (Ig) superfamily and, while sharing low sequence identity, have a common domain structure and interact with receptors belonging to the CD28 protein family (Sharpe and Freeman, 2002; Hansen et al., 2009). In vivo, tissue localization and timing of expression of these molecules provide mechanisms for the fine-tuning of T cell activity in response to a wide range of immune challenges.

B7-H3 is a recently recognized member of the B7 family. Like other members, murine B7-H3 is a type 1 transmembrane protein possessing an ectodomain composed of a single IgV-IgC domain pair with an overall sequence identity of $\leq$30%, when compared to the other B7 family members. In the mouse, B7-H3 transcripts are found in a variety of tissues, including brain, lung, colon, kidney, and spleen (Sun et al., 2002, 2003; Ling et al., 2003). Although initially identified as an activator of T cell function (Chapoval et al., 2001), subsequent reports have shown that B7-H3 can lead to downregulation of T cell activity (Suh et al., 2003; Prasad et al., 2004).

B7-H3 protein is normally found at low levels in many healthy tissues as well as on activated cells of the immune system and has been reported to be strongly overexpressed in a wide variety of human malignancies (Zang et al., 2007; Yamato et al., 2009; Barach et al., 2010; Crispen et al., 2008; Roth et al., 2007; Loos et al., 2010)—a scenario associated with poor clinical outcomes. In particular, 93% of prostate cancers overexpress B7-H3, and patients with higher levels of B7-H3 on tumor cells are significantly more likely to exhibit disseminated disease at the time of surgery, increased recurrence, and higher mortality (Zang et al., 2007). In addition to cancer cells, B7-H3 is also expressed in the endothelium of cancer-associated vasculature in 44% of patients with ovarian cancer, which is associated with a significantly shorter survival time and a higher incidence of recurrence (Zang et al., 2010). These findings, together with the ability

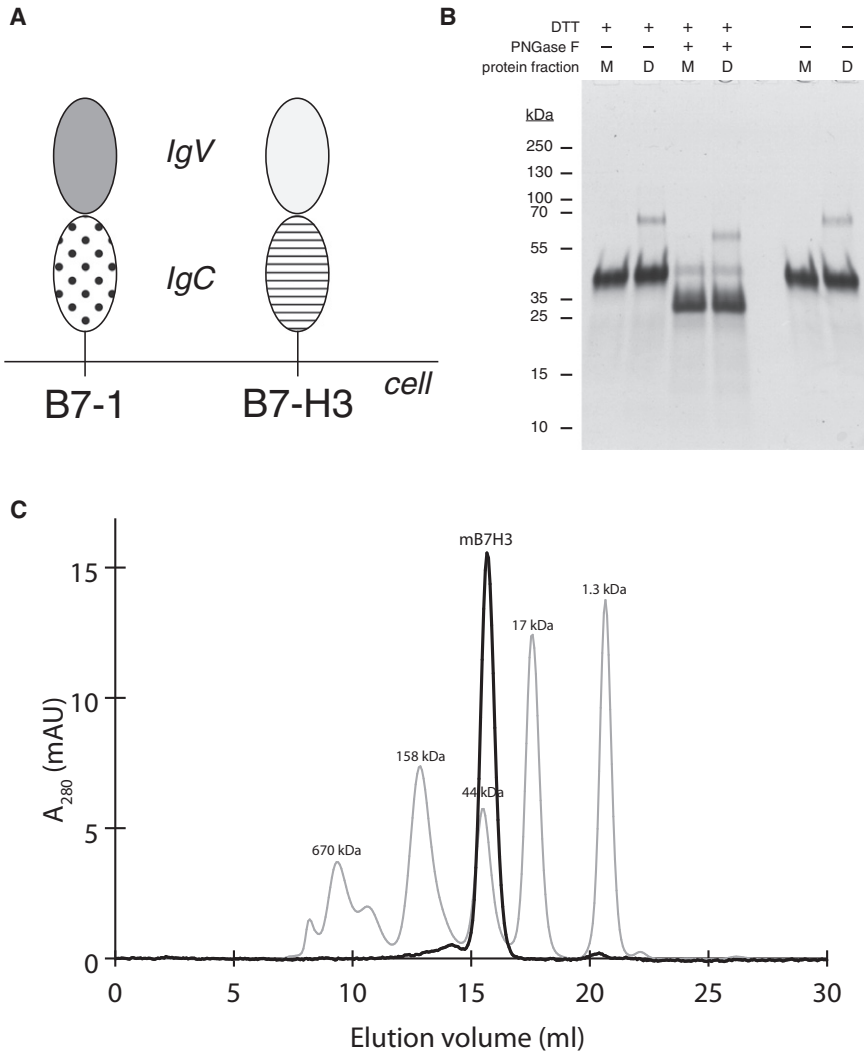


Figure 1. Expression and Purification of mB7H3

(A) Domain organization of murine B7 family members. Diagrams of murine B7-1 and B7-H3 are shown as the representative members of the B7 family. Molecules are expressed as type 1 transmembrane proteins, consisting of an N-terminal IgV and a C-terminal IgC domains, followed by a single transmembrane sequence and a short cytoplasmic tail.

(B) Purified mB7H3 monomer and dimer species are glycosylated and do not contain interchain disulfide bonds. SDS-PAGE of purified monomer (M) and dimer (D) forms of mB7H3 were separated in the presence or absence of dithiothreitol and before and after treatment with PNGase F, as indicated above the lanes.

(C) Native mB7H3 expressed by *Drosophila* S2 cells behaves as a monomer in SEC. Purified protein elutes as a monodisperse peak of ~40 kDa on a calibrated Superdex 200 size-exclusion column (dark trace). Molecular weight standards are shown (light trace). mAU, milliabsorbance unit.

of B7-H3 to inhibit the activity and proliferation of T cells, suggest that tumor cells use the signal delivered by B7-H3 to evade antitumor immunity. The potential role in immune evasion makes B7-H3 a compelling target for anticancer therapy.

We report the crystal structure of the extracellular domain of murine B7-H3, which reveals an unusual organization involving a strand swap between the dimer-forming IgV domains. Based on this structure, a model of B7-H3 with canonical interactions between the IgV and IgC domains was constructed and used as the basis for mutagenesis studies that revealed a critical role for the FG loop of the IgV domain in the ability of mB7H3 to inhibit naive T cell proliferation in vitro. Our findings provide insights for the structure-guided design of the next-generation cancer immunotherapeutics.

RESULTS

mB7H3 Is Produced by *Drosophila* S2 Cells as a Glycosylated Monomer

B7 family members share low sequence identity but possess a common domain structure (Figure 1A) and have a similar mode of interaction with receptors belonging to the CD28 protein family. The ectodomain of murine B7-H3 is composed of a single IgV-IgC domain pair (amino acids 34–247) and was produced as a secreted His_6-tagged protein (mB7H3) using Schneider 2 (S2) *Drosophila* cells. Although the predicted molecular weight of mB7H3 was 24 kDa, purified protein behaved as an ~40 kDa species (Figure 1B) in SDS-PAGE, indicating the presence of glycan modifications at some of the four predicted N-linked glycosylation sites (N91, N104, N189, and N215). The presence of glycans was verified by digestion with peptide N-glycosidase F (PNGase F), which resulted in the reduction of the molecular weight of the mB7H3 to ~30 kDa (Figure 1B). Native protein eluted as an ~40 kDa species in a size-exclusion chromatography (SEC) column (Figure 1C). Taken together, these data indicate that mB7H3 is expressed as a glycosylated monomer.

Crystal Structure of mB7H3

To define the oligomeric organization of mB7H3 and predict its receptor-binding surfaces, we determined its crystal structure (Table 1). The mB7H3 crystals exhibited diffraction consistent with the space group $P6_122$ (a = 100.9 Å, b = 100.9 Å, c = 188.2 Å; one molecule per asymmetric unit), which extended to 2.97 Å. The final refined model accounts for residues 35–151 and 157–239 of mB7H3 with residues 152–156 omitted from the model due to poorly defined electron density, whereas residues 240–247, although present in the expression construct, were not observed in the electron density.

Pairs of mB7H3 molecules related by crystallographic 2-fold axes form extensive contacts, arising from the mutual exchange

 ©2013 Elsevier Ltd All rights reserved

Table 1. Crystallographic Statistics

Data Collection	
Space group	P 6_122
Unit cell	
a (Å)	100.9
b (Å)	100.9
c (Å)	188.2
α (°)	90
β (°)	90
γ (°)	120
Wavelength (Å)	0.9789
Resolution (Å)	50.96–2.97
R_{merge} (%)[a]	11.7 (80.0)
I/σ (I)[a]	18.1 (3.9)
Completeness (%)[a]	99.7 (100.0)
Redundancy[a]	13.1 (13.7)
Refinement	
No. of Reflections	11,661
R_{work} (%)	21.6
R_{free} (%)	25.0
No. of Atoms	
Protein	1,526
Water	5
B Factors (Å^2)	
Protein	72.28
Water	59.03
Rmsd from Ideal Geometry	
Bond lengths (Å)	0.012
Bond angles (°)	1.7

$R_{merge} = \Sigma\ |I - \langle I \rangle| / \Sigma I$, where I is the integrated intensity of a given reflection.
$R_{work} = \Sigma\ ||F_{obs}| - |F_{calc}|| / \Sigma\ |F_{obs}|$.
R_{free} was calculated using 5% of data omitted from refinement.
[a]The highest-resolution shell is shown in parentheses.

of the IgV domains between the neighboring molecules (Figure 2A). The segment connecting F and G strands (the FG loop) of the IgV domain (residues 135–138) adopted an extended "β strand-like" conformation—supported by unambiguous electron density (Figure 2B; Figure S1 available online)—in contrast to the turn-like FG loop conformation found in the classical IgV domain structures. As a result, the IgV domain of dimeric mB7H3 consists of a β sandwich composed of a "back sheet" (BED) and a "front sheet" (C″C′CFG*), the latter of which includes the G* strand contributed by the second protomer.

The C-terminal IgC domain (residues 140–239) consists of a typical β sandwich composed of sheets ABED and CFG (Sun and Boyington, 2001). Topologically, this places both IgC domains on the opposite ends of the elongated mB7H3 dimer, with the C termini separated by ~155 Å.

The mB7H3 sequence contains four potential glycosylation sites: N91, N104, N189, and N215. Electron density that could be interpreted as a single N-acetyl glucosamine (NAG) moiety was present near N91. In the case of N104, three well-ordered sugar residues were observed, corresponding to two NAG and two mannose units. Notably, the location of the glycans on the mB7H3 IgV domain corresponds to the domain's back sheet, consistent with the hypothesis that the front sheet engages the receptor, as shown for other B7 family members.

Although the dimer assembly observed in the crystals is stable in solution (see below), mB7H3 was initially purified as a monomer (Figure 1C), which is likely the dominant form present on the cell surface. To generate a model of the monomeric form of mB7H3, we built a "hybrid" model consisting of residues 35–125 from one protomer and residues 130–238 from its 2-fold symmetry-related mate (Figure 2C); predicted FG loop residues (126–129) were modeled as a β turn using the ArchPRED software (Fernandez-Fuentes et al., 2006). The resulting monomeric mB7H3 model aligns well with a representative B7 family member structure—i.e., human PD-L1 (Protein Data Bank [PDB] 3BIK, chain A; overall C_α rmsd ~2.7 Å, IgV C_α rmsd ~1.1 Å; Figure 2D)—indicating that the overall organization of the proposed mB7H3 monomer is consistent with those of other B7 family members.

The FG Loop Is Important for mB7H3-Mediated Inhibition of T Cell Proliferation

Guided by the receptor-binding properties of other Ig superfamily members and the model of monomeric mB7H3, we generated a panel of mutants targeting the surface residues of the front sheet of the N-terminal IgV domain, including the FG loop (Figure 3B). This surface has been shown to play a critical role in receptor recognition for a number of B7 family members, including B7-1 (Stamper et al., 2001), B7-2 (Schwartz et al., 2001), PD-L1 (Lin et al., 2008), and PD-L2 (Lázár-Molnár et al., 2008).

B7-H3 function has been previously evaluated in T cell proliferation assays (Chapoval et al., 2001; Suh et al., 2003; Prasad et al., 2004). In our assay, purified proteins were immobilized on plastic tissue culture plates in the presence of monoclonal anti-murine-CD3 antibody (which was used to engage the TCR-mediated "signal 1"). To ensure a homogeneous T cell activation state, TCR-transgenic OT-II cells were used in these experiments. $CD4^+$ T cells, freshly isolated from OT-II mice, were incubated in these plates to compare cell proliferation in the presence of wild-type (WT) or mutant mB7H3 proteins (the optimal mB7H3 concentration was determined, as shown in Figure 3A). To eliminate possible complications associated with mB7H3 dimers, freshly purified protein stocks were kept at concentrations below 2 mg/ml (details of mB7H3 dimerization are described below).

The presence of WT mB7H3 consistently resulted in an ~50% decrease in T cell proliferation compared to control conditions (PBS or rat IgG), indicating that mB7H3 delivered a signal that was inhibitory to T cells (Figure 3C). In this assay, the greatest effect was associated with the exchange of the B7-H3 FG loop sequence with the corresponding sequence from human PD-L1. This chimeric FG loop mutant (I126Y/Q127G/D128G/F129A) showed a consistent and significant ($p < 0.05$) difference with respect to the WT mB7H3, resulting in a nearly complete loss of inhibitory activity (Figure 3C). In contrast, FG loop point mutants I126T and F129A were not significantly different from WT mB7H3. Surprisingly, none of

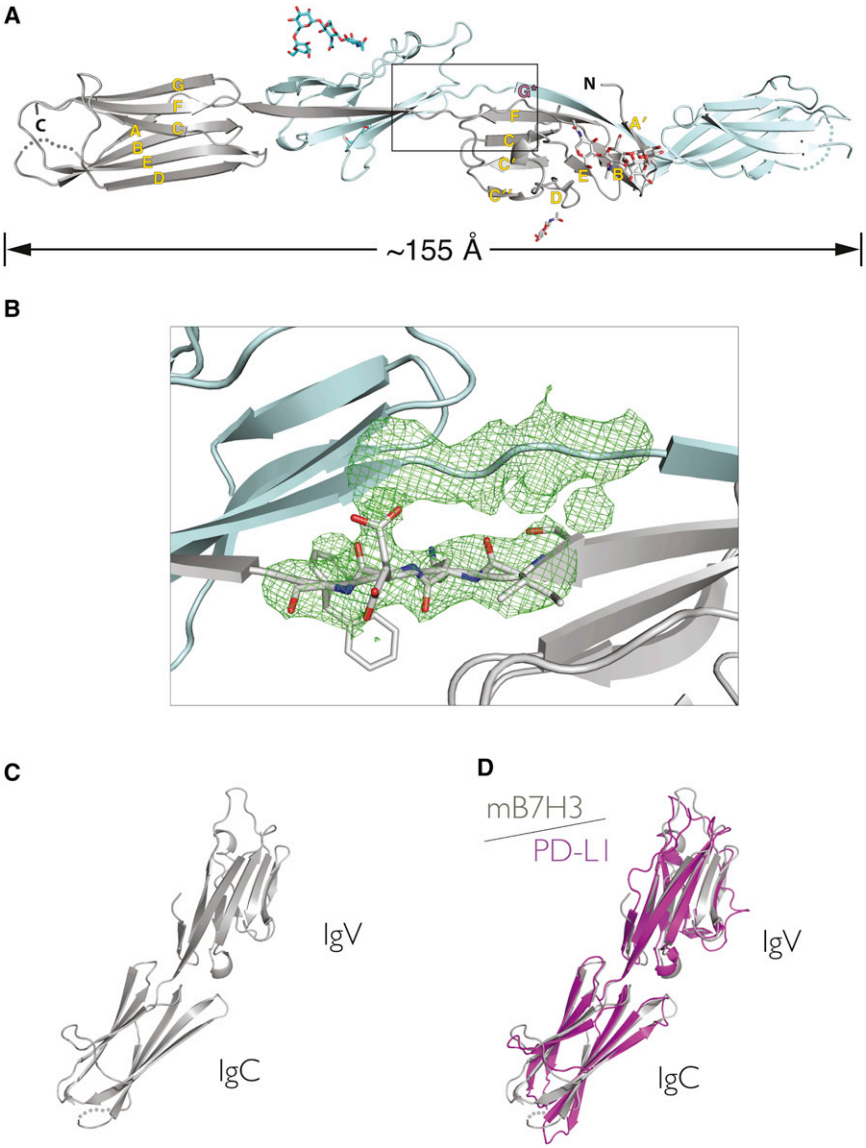


Figure 2. Structure of mB7H3

(A) Crystals of mB7H3 contain the dimeric form of the protein. Ribbon representation of the crystallographic dimer of mB7H3 with each protomer drawn in different colors (gray and cyan) with N and C termini labeled for one of the protomers. Unmodeled residues 152–156 of the IgC domain of each protomer are shown with dots of corresponding color. The glycans (two on each protomer) are drawn in stick representation. Strands making up the Ig fold in each domain are labeled in yellow, whereas the strand exchanged between the two protomers (G*) is labeled in pink.

(B) Electron density of the extended FG loop-bridging sequence. *Fo*−*Fc* electron density map, calculated with the FG loop sequence omitted, contoured at +3σ is shown in green near the location of the strand exchange highlighted by a box in (A). Ribbon diagrams representing the structure for each mB7H3 protomer are shown. The side chains of the FG loop residues are shown in gray stick-figure representation.

(C) Structure-based model of monomeric mB7H3. Model of the mB7H3 monomer was constructed by combining residues 35–125 from one protomer and residues 130–238 from its 2-fold-related symmetry mate.

(D) Monomeric model of mB7H3 corresponds well to the PD-L1 structure. Structural alignment (overall C_α rmsd ~2.7 Å) of the monomeric mB7H3 model (gray) and the structure of human PD-L1 (purple).

See also Figure S1.

the point mutants that targeted the front sheet of the mB7H3 IgV domain resulted in a statistically significant change in OT-II T cell inhibition. Similar data were obtained using $CD4^+$ T cells isolated from C57BL/6 mice (which express a normal T cell repertoire, in contrast to OT-II mice), with the exception of the T121A mutant, which was significantly impaired in its inhibitory function compared to WT mB7H3 (Figure S2). Taken together, these data show that receptor recognition by B7-H3 involves the residues of the FG loop but that mutation of individual front sheet residues to alanine is insufficient to disrupt its T cell inhibitory function.

B7-H3 Does Not Bind TLT-2

The identity of the receptor(s) responsible for the T cell coinhibitory and costimulatory effects of B7-H3 has not been conclusively established. Although expression of the triggering receptor expressed on myeloid cell (TREM)-like transcript-2 (TLT-2) has been reported to specifically bind B7-H3 and result in B7-H3-dependent T cell stimulation (Hashiguchi et al., 2008), these findings could not be reproduced in similar experimental systems using murine or human cells (Leitner et al., 2009). To address these discrepancies, we expressed the ectodomain of murine TLT-2 as a secreted His_6-tagged protein (mTLT2) using S2 cells and found that mTLT2 and mB7H3 did not bind to each other in SEC or surface plasmon resonance experiments (data not shown). Furthermore, murine B7-H3 Ig fusion could not bind TLT-2-expressing cells in flow cytometry experiments (data not shown). These observations suggest that TLT-2 is not a binding partner for B7-H3.

mB7H3 Forms a Stable Dimer upon Extended Incubation at High Protein Concentration

Stock solutions of purified mB7H3 used in crystallization experiments were routinely concentrated to >10 mg/ml and stored at 4°C. Following extended storage (>3 weeks), we observed a time- and concentration-dependent accumulation of a high molecular weight protein species by SEC (Figures 4A and 4B). This SEC peak eluted at a volume corresponding to a protein of ~80 kDa—double that of monomeric mB7H3—and did not revert to the original SEC elution profile (corresponding to ~40 kDa) following purification and dilution (data not shown).

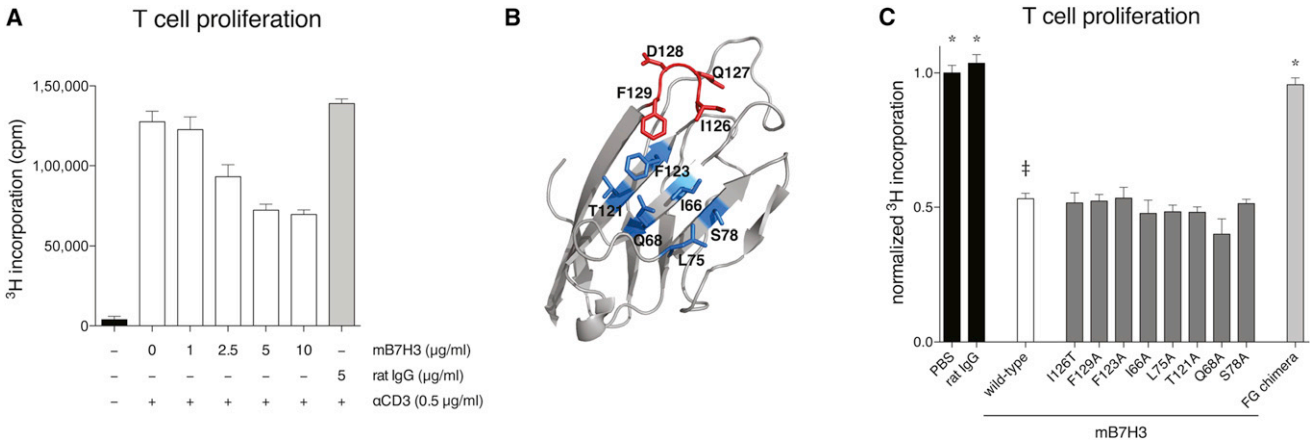


Figure 3. Functional Characterization of mB7H3 Wild-Type and Mutants

(A) CD4$^+$ T cell proliferation is inhibited by mB7H3 in a dose-dependent manner. CD4$^+$ OT-II cells were cultured in plasticware pretreated with the proteins indicated below the x axis. T cell proliferation was assayed by pulsing with [^{3}H]thymidine during the last 18 hr of a 3 day incubation. Average values obtained from four replicates are shown with error bars representing the SEM.

(B) Mapping of front sheet and FG loop mutations on the structure of mB7H3. The N-terminal IgV domain of mB7H3 monomer is shown in ribbon diagram (gray). Residues of the FG loop (red) and mutated front sheet positions (blue) are labeled and shown with side chains represented as stick figure.

(C) T cell proliferation is inhibited by WT, but not the FG loop chimera of mB7H3. CD4$^+$ OT-II T cells were cultured in 96-well plates precoated with 0.5 μg/ml anti-CD3 and 5 μg/ml proteins indicated along the x axis. T cell proliferation was assayed by pulsing with [^{3}H]thymidine during the last 18 hr of a 3 day incubation. Data were normalized to the mean value obtained for anti-CD3 alone (PBS). Average values obtained from two experiments (four replicates per sample per experiment) are shown with error bars representing the SEM. Statistically significant differences ($p < 0.05$, ANOVA) with respect to the WT mB7H3 sample (double dagger) are labeled with asterisks.

See also Figure S2.

SDS-PAGE analysis indicated that this protein species was indistinguishable from the original mB7H3 sample, when denatured (Figure 1B). Furthermore, the complex was found to contain no interchain disulfide bonds when separated under nonreducing conditions (Figure 1B).

To identify the physicochemical properties responsible for mB7H3 dimer formation, we subjected monomeric mB7H3 to a range of ionic strengths, redox conditions, pHs, and temperatures. None of the conditions tested promoted dimer formation (data not shown).

Dimerization of mB7H3 Is Perturbed by Mutations in the FG Loop

The four-residue sequence I(Q/R)DF (126–129) of the FG loop in B7-H3 is conserved among the mammalian B7-H3 sequences (Figure 5A). It is also strikingly different from the corresponding YGGA sequence, conserved in the homologous murine PD-L1 (Figure 5B), structure of which has been previously reported (PDB 3BIK, 3BIS, 3SBW, and 3FN3). Based on the fact that in our structure, the FG loop sequence adopts a strand-like conformation, we hypothesized that it may play a role in mB7H3 dimerization. To assess this possibility, we monitored the dimerization of mutants I126T, F129A, and the FG loop chimera (I126Y/Q127G/D128G/F129A) (Figure 6A).

Each mutant was expressed and purified using the S2 *Drosophila* system described above, and dimer formation was evaluated by SEC, as described for the WT mB7H3. Compared to that of WT mB7H3, dimer formation was significantly slower for mutants I126T and the FG loop chimera, whereas mutant F129A exhibited behavior similar to the WT mB7H3 (Figure 6B; Table 2).

Both Monomeric and Dimeric mB7H3 Inhibit the Proliferation of CD4$^+$ T Cells

In order to determine whether dimerization plays a role in mB7H3 function, we compared monomeric mB7H3 to predimerized samples in the T cell proliferation assay described above. Freshly purified protein stocks were kept at concentrations below 2 mg/ml to prevent mB7H3 dimerization, and the dimeric samples were verified to be stably dimeric over the course of the experiments (data not shown).

As described above, WT monomeric mB7H3 caused a consistent ~50% decrease in T cell proliferation compared to control conditions (PBS or rat IgG), indicating that mB7H3 delivered an inhibitory signal to the T cells (Figure 6C, "WT monomer"), whereas the replacement of the FG loop caused near loss of the inhibition (Figure 6C, "FG chimera"). In order to test the dimeric form of mB7H3, a sample undergoing dimerization and containing ~40% mB7H3 dimer was separated by SEC, and the resulting monomer and dimer fractions were tested (Figure 6C, samples "WT monomer*" and "WT dimer*"). We found that dimeric mB7H3 did not significantly differ from the monomeric form in its ability to inhibit T cell proliferation. This indicates that dimerization of mB7H3 alone does not alter the inhibitory property on the molecule.

DISCUSSION

B7-H3 Structure

Here, we present the structure of the murine B7-H3 ectodomain, which reveals a noncanonical quaternary structure previously described for other members of the Ig superfamily. We observed mB7H3 dimers formed by an unusual strand/domain swap

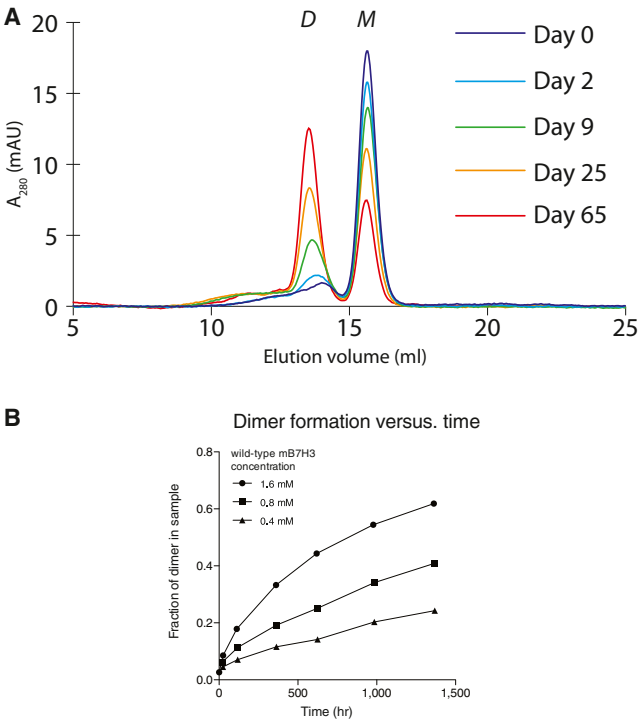


Figure 4. mB7H3 Forms Stable Dimers in Solution

(A) Purified mB7H3 dimerizes during incubation. Protein samples were concentrated to ~1.6 mM (60 mg/ml) and incubated at 4°C. SEC traces represent experiments carried out at the time points indicated. Monomer (M) and dimer (D) peaks are labeled.

(B) WT mB7H3 dimerizes over time in a concentration-dependent manner. SEC time course data similar to those shown in (A) were obtained for the indicated concentrations of WT mB7H3. Each data point represents the proportion of dimer observed (as measured by dimer peak height) compared to the total (monomer peak height plus dimer peak height).

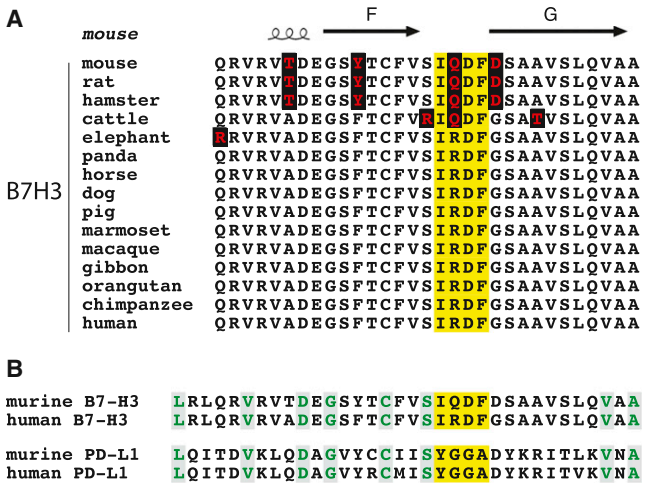


Figure 5. Sequence Conservation of the FG Loop

(A) Sequence of the B7-H3 FG loop is conserved. Clustal W (Larkin et al., 2007; Goujon et al., 2010) was used to align the mB7H3 sequences from eight mammalian species, and the resulting alignment is presented using ESPript (Gouet et al., 1999). Secondary structural elements of the mB7H3 structure are labeled (top line). Sequence differences are shown as red lettering on black background. The four FG loop residues are highlighted with yellow background.

(B) Sequence of the FG loop is divergent between B7 family members. Clustal W (Larkin et al., 2007; Goujon et al., 2010) sequence alignment of murine and human sequences of B7-H3 and PD-L1 is shown. Positions identical in all sequences are shown in green lettering with gray background. The four FG loop residues are highlighted with yellow background.

between partner molecules (Figure 2A), resulting in an elongated assembly with the C termini separated by ~155 Å. Notably, crystals formed only from protein stocks that had been stored for several weeks following purification, while freshly purified samples failed to yield crystals. Furthermore, we did not identify any crystallization conditions for the FG loop chimera, which was severely impaired in its capacity to dimerize (Figure 6B). The dimeric arrangement is stabilized by the exchange of the F strands in the partner molecules within the IgV fold of the N-terminal domain. The sequence connecting the F and G strands, which normally forms the FG loop, is fully extended in the dimer and forms a short two-stranded bridge between the two protomers. This organization is distinct from the typical mode of dimerization in the Ig superfamily, which involves contacts between the two front sheets of the IgV domains from interacting partner molecules (reviewed in Chattopadhyay et al., 2009).

Nevertheless, similar dimers have been described for at least three other members of the Ig superfamily: the llama antibody VHH-R9 domain (Spinelli et al., 2004); the human CD47 IgV domain (Hatherley et al., 2008); and the CTLA-4 IgV domain (Sonnen et al., 2010) (Figure 7). According to these reports, dimer formation was not detected in solution, although all of these molecules crystallized as dimers linked by the swap of the G strand (similar to the mB7H3 structure reported here). In addition, CTLA-4 IgV domain spontaneously forms amyloid aggregates.

In addition to yielding the structure of the dimeric form of mB7H3, our data provided us with a plausible model of its monomeric precursor (Figure 2C). In particular, the overall superposition of the mB7H3 monomeric model and the human PD-L1 structure (3BIK) demonstrates that the individual IgV and IgC domain folds, as well as their positions with respect to one another, align well (Figure 2D). This observation suggests that the invading G strand from each of the protomers occupies a position in the accepting IgV domain of its partner molecule that is equivalent to its position in the monomeric precursor.

B7-H3 Function

The precise function of B7-H3 remains unclear because it has been reported to stimulate (Chapoval et al., 2001; Hashiguchi et al., 2008; Kobori et al., 2010), inhibit (Suh et al., 2003; Prasad et al., 2004; Xu et al., 2006; Leitner et al., 2009; Chen et al., 2011), and have no effect (Steinberger et al., 2004) on T cell proliferation in various experimental systems. Understanding the role that B7-H3 plays in immunity is further confounded by the fact that B7-H3-deficient mice are generally healthy and have normal cellular compositions of their immune compartments (Suh et al., 2003), suggesting that the loss of B7-H3 function in these animals can be compensated for by other mechanisms. Nevertheless, most reports to date suggest that T cells express an unidentified receptor(s) that binds to B7-H3, resulting in a modulation of the T cell response to antigen-dependent signals.

 ©2013 Elsevier Ltd All rights reserved

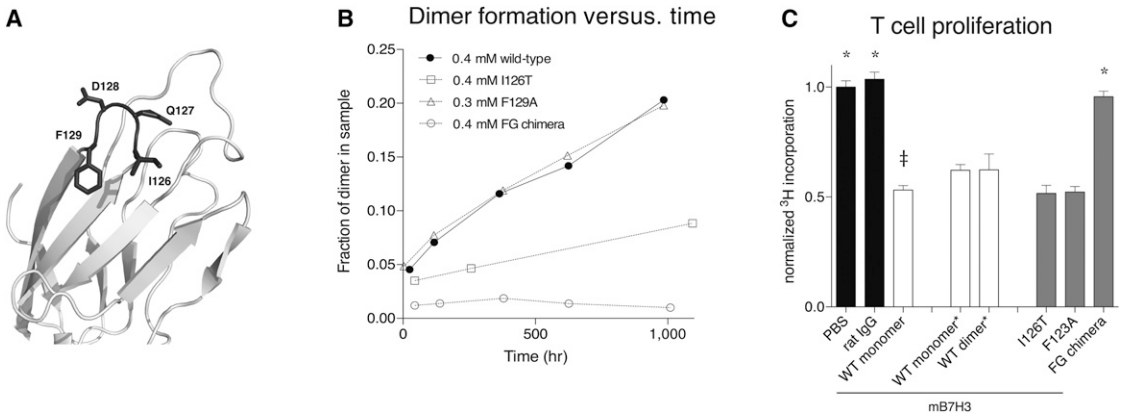


Figure 6. Functional Characterization of mB7H3 Monomer and Dimer

(A) Mapping FG loop mutations on the structure of mB7H3. The N-terminal IgV domain of mB7H3 monomer is shown in ribbon diagram (gray). Residues of the FG loop (black) are labeled and shown with side chains represented as stick figures.

(B) Mutations at the FG loop disrupt dimerization of mB7H3. Dimer formation was measured for mB7H3 FG loop mutants using experiments similar to those shown in Figure 4A.

(C) T cell proliferation is inhibited by monomeric and dimeric WT, but not the FG loop chimera of mB7H3. $CD4^+$ OT-II cells were cultured in 96-well plates precoated with 0.5 μg/ml anti-CD3 and 5 μg/ml of the proteins indicated along the x axis. T cell proliferation was assayed by pulsing with [^{3}H]thymidine during the last 18 hr of a 3 day incubation. Data were normalized to the mean value obtained for the treatment with anti-CD3 alone (PBS). Average values obtained from two experiments (four replicates per sample per experiment) are shown with error bars representing the SEM. Statistically significant differences ($p < 0.05$, ANOVA) with respect to the WT mB7H3 sample (double dagger) are labeled with asterisks.

In order to study the biological activity of mB7H3, we tested purified protein samples in an in vitro system similar to those described earlier by Prasad et al. (2004), Hashiguchi et al. (2008), and Suh et al. (2003). Although we initially used C57BL/6-derived T cells, we found that the experimental variation was significantly lower with the cells isolated from OT-II mice. Despite the differences, the data from these two mouse strains were, generally, in agreement. $CD4^+$ T cells isolated from either C57BL/6 or OT-II mice showed a reproducible ~50% inhibition of proliferation when cultured in tissue culture plates pretreated with a combination of anti-CD3 and WT mB7H3, compared to control conditions (anti-CD3 alone or in combination with an irrelevant protein) (Figures 3C and S2). Thus, in our system, we observed that B7-H3 plays an inhibitory role in T cell activation.

Based on the similar modes of receptor recognition among the B7 family members (Lázár-Molnár et al., 2008; Lin et al., 2008; Stamper et al., 2001; Schwartz et al., 2001), we hypothesized that the residues located on the surface of the front sheet of the IgV domain are involved in recognition of the B7-H3 receptor. A number of mutants on the front sheet surface (I126T, F129A, F123A, I66A, L75A, T121A, Q68A, S78A) had inhibitory activities that could not be distinguished from that of WT mB7H3 using the OT-II cells (Figure 3C) or the C57BL/6-derived cells (with the exception of the T121A mutant, which showed a significant impairment) (Figure S2). Taken together, our data suggest that either the individual contributions of these residues are insufficiently strong to be detected in our assay or that this molecular surface does not make major contributions to recognition by the receptor.

In contrast, simultaneous multiple mutations resulting from the replacement of the FG loop with the corresponding sequence from murine PD-L1 (FG chimera) resulted in a nearly complete loss of inhibition of OT-II cells (Figure 3C) and a significant impairment of inhibition of C57BL/6-derived cells (Figure S2). These data indicate that the FG loop residues are involved in B7-H3 interaction with the receptor expressed on T cells.

Recombinant B7-H3 Dimerization

We demonstrated that mB7H3 spontaneously dimerizes under physiologic pH and ionic strength. This behavior raises questions as to whether the mB7H3 dimer represents a physiologically significant species. In particular, how can the slow kinetics support significant dimer formation in vivo? At least three hypotheses emerge: (1) topological restrictions imposed by the association with the plasma membrane of interacting cells may provide a stabilizing environment during monomer/dimer transition under physiologic conditions; (2) additional membrane-associated molecules facilitate the process of mB7H3 dimer formation on the cell surface or in an intracellular compartment; or (3) the crystallographically observed mB7H3 dimer may be an in vitro artifact with no in vivo correlate.

Based on the comparison between the model of the mB7H3 monomer and the observed dimer structure, we hypothesized that the sequence connecting the strands F and G of the IgV domain can adopt at least two conformations (extended and β turn-like) and thus plays a role in the ability of B7-H3 to dimerize. To address this hypothesis, we generated a series of mutants targeting the loop connecting the F and G strands. Introduction of the FG loop sequence (YGGA) from PD-L1, containing the highly flexible Gly-Gly pair of residues, severely impaired dimer formation with an ~18-fold reduction in the rate of dimerization.

Additionally, when modeled in the β turn conformation (i.e., in the monomeric form), the predicted geometry of the mB7H3 FG loop would cause the hydrophobic residue Ile-126 to be more solvent exposed, than in the extended conformation observed in dimeric mB7H3. In the latter case, the Ile-126 side chain

Table 2. Dimerization Kinetics of mB7H3 and Mutants

Mutation	FG Loop Sequence	Association Rate Constant $\times 10^{-5}$ (l/mol/s)
WT	IQDF	16.1 ± 0.6
I126T	TQDF	4.1 ± 0.1
F129A	IQDA	16.4 ± 0.3
FG chimera	YGGA	0.83 ± 0.08

Values were determined using the fitting analysis shown in Figure S3.

interacts more tightly with the hydrophobic side chains of Phe-52 and Phe-58, stabilizing the extended conformation of the mB7H3 protomer and the dimer itself. Introduction of the I126T mutation in mB7H3 resulted in an ~3-fold reduction in the dimerization rate, supporting the hypothesis that hydrophobicity of Ile-126 contributes to dimer formation. Taken together, our analysis of the FG loop in mB7H3 suggests that the WT sequence may play a destabilizing role for the monomeric form of mB7H3.

Implications of B7-H3 Dimerization for Biological Function

The functional relevance of strand-swapped dimer formation among the Ig superfamily members is not clear. Of the known examples, strand exchange of the llama antibody VHH domain would render it incapable of engaging antigen due to the remodeling at the antigen-binding site. In CD47, the N-terminal IgV domain is topologically constrained with respect to the C-terminal portions of the molecule, making it unlikely to participate in the strand-swap dimerization while expressed on the cell surface. On the other hand, amyloid fiber formation by CTLA-4 suggests a potential mechanism by which strand swapping may lead to a variety of diseases associated with Ig deposition (Bennett et al., 2006). Although B7-H3 has not been implicated in amyloid-caused disease, our data lend credence to the notion that IgV domains may exhibit unanticipated plasticity.

The B7-H3 dimer structure reported here positions the transmembrane regions of the molecule at an ~155 Å distance. This arrangement is suggestive of a mechanism by which homophilic B7-H3 interactions may bridge two interacting cells and may possibly represent a ligand:ligand or a ligand:receptor complex (in which case, one or both of the B7-H3 molecules would facilitate signaling to its parent cell). Interestingly, our structure predicts that if the front sheet of the B7-H3 IgV domain is involved in receptor recognition, the binding surface would be accessible in the dimeric form of B7-H3. Furthermore, in our experiments, the mB7H3 dimer had the same inhibitory activity as the monomer in the T cell proliferation assay (Figure 6C), which is consistent with this notion. However, due to the slow rate of mB7H3 dimer formation measured in solution (Table 2), it is likely that additional mechanisms are involved in facilitating B7-H3 dimerization, if it plays a role in B7-H3 function.

Finally, we have shown that the inhibitory activity of mB7H3 FG chimera is severely impaired and that this mutant is also impaired in its ability to dimerize in solution. Although these observations are intriguing, we believe that they are unlikely to be related for the following reasons: (1) the monomeric and dimeric forms of mB7H3 are functionally equivalent in our T cell proliferation assays (Figure 6C), and (2) the I126T mutant is functional in the T cell proliferation assays (Figures 6C and S2) but is significantly impaired in its dimerization properties (Figure 6B). Thus, our data lead us to conclude that whereas both conformations of the FG loop are equally functional, the identities of the residues of the FG loop are critical for receptor recognition.

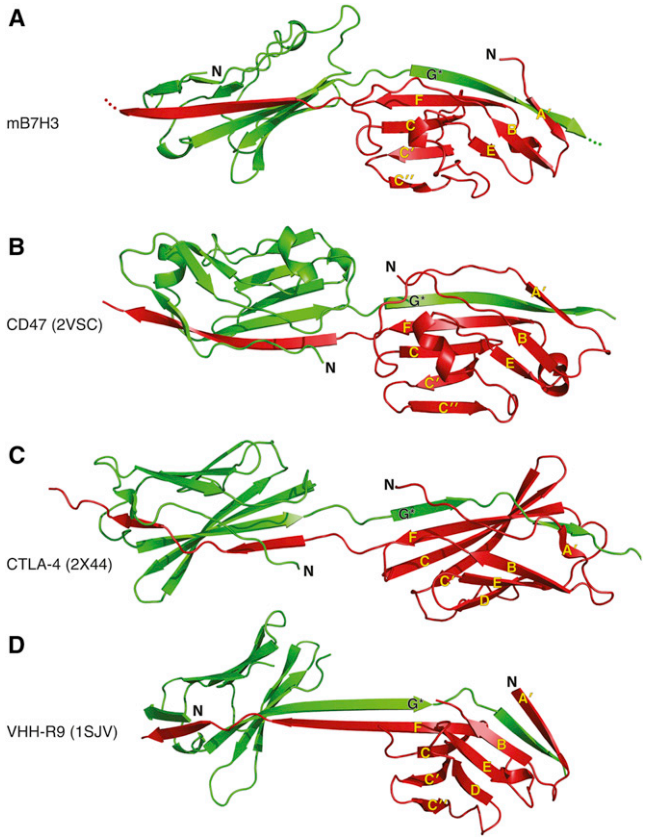


Figure 7. Strand-Swapped Dimer Formation among the Members of the Ig Superfamily

Structures of strand-swapped dimers of IgV domains. N-terminal IgV domain dimer of mB7H3 (A), CD47 (B), CTLA-4 (C), and llama VHH-R9 Ig (D). Each protomer is labeled in different colors (green and red), with N termini labeled. Strands making up the two β sheets of the Ig fold are labeled (yellow), and the swapped strand (G*) is labeled in black.

In summary, we determined the structure of murine B7-H3 and used it to characterize the molecular determinants responsible for receptor recognition. A growing body of literature suggests that B7-H3 is a key factor in the progression of many cancers and highlights the importance of studies of the biology of this molecule as well as its binding partners, which control the immune response at tumor sites. Although the precise role that B7-H3 plays in in vivo T cell regulation remains to be defined, we demonstrated that it has a clear inhibitory function in our assay system and identified the FG loop sequence in its IgV domain as important for this function. The development of therapeutics specifically targeting this sequence may prove useful as an anticancer drug strategy.

 ©2013 Elsevier Ltd All rights reserved

EXPERIMENTAL PROCEDURES

DNA Cloning

DNA encoding the predicted extracellular fragment of murine B7-H3 (amino acids 34–247) was amplified by PCR using primers containing BglII and AgeI restriction sites and cloned into the pMT/BiP/V5-His A (Invitrogen) or the pCGMbX vectors, which includes a constitutively expressed *egfp* gene. Constructs containing mutations of single residues and contiguous spans were generated using QuikChange Site-Directed Mutagenesis Kit (Stratagene).

Cell Lines

Express Five SFM (Invitrogen) was used for routine culture and recombinant protein expression using *Drosophila* S2 cells. Schneider's *Drosophila* Medium (Invitrogen), supplemented with 10% fetal bovine serum, was used when transfecting the cells using the calcium phosphate method (Invitrogen). Alternatively, transfection was performed using the dimethyl dioctadecyl ammonium bromide (DDAB) method (Han, 1996) in Express Five SFM. Following cotransfection of the target-containing vector and the selection vector (pCoBlast or pCoPuro; mixed at a ratio of 1:20 with the target-containing vector), the cells were allowed to recover for ~48 hr before being selected with either 25 μg/ml Blasticidin S (Invitrogen) or 10 μg/ml puromycin (Fisher). To improve protein expression, drug-resistant cell populations were subcloned using a modified version of the limited dilution method by Yang et al. (2004). Briefly, parental S2 feeder cells were irradiated (20,000 rads) and coplated with target stable cell populations at a ratio of 250,000:3 (feeder:target) per well of a 96-well plate. The target cells were allowed to form colonies over the course of 2–3 weeks while being supplemented with fresh medium every 4–6 days. The colonies were then resuspended and replica plated into an induction plate containing fresh medium supplemented with 1 mM copper sulfate. Following a 7 day incubation, the supernatants from the induction plate were screened by dot blot using Penta-His antibody (QIAGEN) to identify the high expressors among the stable cell line populations.

Animals

C57BL/6 and OT-II mice were purchased from The Jackson Laboratory (Bar Harbor, ME, USA) and maintained under pathogen-free conditions at the Albert Einstein College of Medicine. OT-II mice carry an MHC class II-restricted chicken ovalbumin-specific TCR transgene, thus narrowing the specificity of their entire T cell repertoire to just this antigen. Mice were used in the experiments at 6–12 weeks of age. All animal work was performed according to the guidelines set by the Institutional Animal Care and Use Committee.

Protein Expression and Purification

Cell lines were expanded in shaker-flask suspension cultures and induced with 1 mM copper sulfate. Cultures were harvested 7 days postinduction, centrifuged to remove cells and debris, supplemented with 150 mM NaCl and 0.02% sodium azide, and filtered using 0.22 μm membrane. The resulting clarified supernatants were flowed over a column containing Ni-NTA agarose (QIAGEN), washed with TBS (20 mM Tris-HCl [pH 8], 300 mM NaCl, 0.02% sodium azide), TBS plus 20 mM imidazole, and eluted using TBS plus 200 mM imidazole. Eluted protein was concentrated and further purified using gel filtration on Superdex 200 resin in HBS-E buffer (20 mM HEPES [pH 7], 150 mM NaCl, 1 mM EDTA).

Crystallization, Data Collection, and Modeling

Diffraction-quality crystals were grown in sitting-drop crystallization reactions containing 1 μl of protein solution (10 mg/ml in HBS-E) and 1 μl reservoir solution (0.1 M HEPES [pH 7.5] and 20% polyethylene glycol 10,000 [w/v]). Crystals were cryoprotected in reservoir solution supplemented with 20% ethylene glycol (v/v) prior to flash cooling in liquid nitrogen. X-ray diffraction data were collected at beamlines 24-ID-E (Advanced Photon Source, Argonne, IL, USA) and X29 (National Synchrotron Light Source, Upton, NY, USA).

Data were integrated using the iMOSFLM (Battye et al., 2011) software with subsequent processing using the programs within the CCP4 software package (Winn et al., 2011). An initial structure, based on the structure of human PD-L1 (PDB 3BIK), was determined using the BALBES software package (Long et al., 2008). The model was further built using Coot (Emsley et al., 2010) and refined using REFMAC5 (Murshudov et al., 1997).

Dimerization Kinetics Measurements

Concentrated WT and mutant mB7H3 protein stocks were serially diluted in HBS-E buffer and incubated at 4°C. Aliquots containing ~50 μg of protein were separated on a standardized analytical Superdex 200 sizing column, and the peak heights (absorbance at 280 nm) corresponding to monomer and dimer protein species were recorded for the duration of each time course. Concentrations of monomer and dimer species were estimated based on the fraction of peak heights of each component with respect to total protein amount. These data were used to generate a global fit (using data from multiple concentrations of each protein) against a model for a second-order reaction rate law (as shown in Figure S3) using GraphPad Prism (v.5) software to obtain the apparent association rate constants shown in Table 2.

T Cell Proliferation Assays

$CD4^+$ T cells were isolated from the spleens and superficial lymph nodes of 6- to 8-week-old OT-II or C57BL/6 mice using mouse CD4 Dynabeads and DETACHaBEADs (Invitrogen). A total of 2×10^5 purified $CD4^+$ T cells were plated into each well of a 96-well cell culture plate precoated (for 16 hr at 4°C) with 0.5 μg/ml solution of CD3ε antibody (BD Biosciences), also containing the indicated amounts of WT mB7H3 monomer, mB7H3 dimer, mB7H3 mutants, rat IgG2b (BioExpress), as a protein control, or a PBS control. [^{3}H] thymidine (PerkinElmer) was added for the last 18 hr of the 72 hr cultures, and T cell proliferation was measured by detecting ^{3}H incorporation using a Wallac MicroBeta 1450 TriLux Liquid Scintillation Counter. Where indicated, data were normalized with respect to the average signal obtained with anti-CD3/PBS control. Replicates of at least four wells were used for each condition, and the experiments were repeated two to five times. Optimal concentrations of anti-CD3 and monomeric mB7H3—specific to our assay system—were determined by dose-response titration experiments such as the one shown in Figure 3A. The data were analyzed using one-way ANOVA followed by Dunnett's multiple comparison test (GraphPad Prism, v.5); p values < 0.05 were considered significant. For more details, please see Supplemental Experimental Procedures.

ACCESSION NUMBERS

The structure factors and the final model coordinates have been deposited into the Protein Data Bank and have been assigned the accession number 4I0K.

SUPPLEMENTAL INFORMATION

Supplemental Information includes three figures and Supplemental Experimental Procedures and can be found with this article online at http://dx.doi.org/10.1016/j.str.2013.03.003.

ACKNOWLEDGMENTS

The authors gratefully acknowledge Dr. Jeffrey B. Bonanno for helpful discussions during structure determination, Dr. Kaya Ghosh for her contributions to the T cell-based assay setup, Dr. Deborah Palliser for her help with the experimental design, and Dr. Teresa P. DiLorenzo for her insightful suggestions during the writing of this manuscript. This work was supported in part by NIH grants GM094662 (to S.C.A.), GM094665 (to S.G.N.), AI007289 (to S.G.N. and S.C.A.), DP2DK083076 (to X.Z.), and CA009173 and the Irvington Institute Fellowship Program of the Cancer Research Institute (to V.V.), and Department of Defense Grant PC094137 (to X.Z.). The Albert Einstein Cancer Center is supported by NIH P30CA013330.

Received: December 18, 2012
Revised: February 18, 2013
Accepted: March 1, 2013
Published: April 11, 2013

REFERENCES

Barach, Y.S., Lee, J.S., and Zang, X. (2010). T cell coinhibition in prostate cancer: new immune evasion pathways and emerging therapeutics. Trends Mol. Med. *17*, 47–55.

Battye, T.G.G., Kontogiannis, L., Johnson, O., Powell, H.R., and Leslie, A.G.W. (2011). iMOSFLM: a new graphical interface for diffraction-image processing with MOSFLM. Acta Crystallogr. D Biol. Crystallogr. *67*, 271–281.

Bennett, M.J., Sawaya, M.R., and Eisenberg, D. (2006). Deposition diseases and 3D domain swapping. Structure *14*, 811–824.

Chapoval, A.I., Ni, J., Lau, J.S., Wilcox, R.A., Flies, D.B., Liu, D., Dong, H., Sica, G.L., Zhu, G., Tamada, K., and Chen, L. (2001). B7-H3: a costimulatory molecule for T cell activation and IFN-gamma production. Nat. Immunol. *2*, 269–274.

Chattopadhyay, K., Lázár-Molnar, E., Yan, Q., Rubinstein, R., Zhan, C., Vigdorovich, V., Ramagopal, U.A., Bonanno, J., Nathenson, S.G., and Almo, S.C. (2009). Sequence, structure, function, immunity: structural genomics of costimulation. Immunol. Rev. *229*, 356–386.

Chen, W., Hou, Z., Li, C., Xiong, S., and Liu, H. (2011). Cloning and characterization of porcine 4Ig-B7-H3: a potent inhibitor of porcine T-cell activation. PLoS One *6*, e21341.

Crispen, P.L., Sheinin, Y., Roth, T.J., Lohse, C.M., Kuntz, S.M., Frigola, X., Thompson, R.H., Boorjian, S.A., Dong, H., Leibovich, B.C., et al. (2008). Tumor cell and tumor vasculature expression of B7-H3 predict survival in clear cell renal cell carcinoma. Clin. Cancer Res. *14*, 5150–5157.

Emsley, P., Lohkamp, B., Scott, W.G., and Cowtan, K. (2010). Features and development of Coot. Acta Crystallogr. D Biol. Crystallogr. *66*, 486–501.

Fernandez-Fuentes, N., Zhai, J., and Fiser, A. (2006). ArchPRED: a template based loop structure prediction server. Nucleic Acids Res. *34*(Web Server issue), W173–W176.

Gouet, P., Courcelle, E., Stuart, D.I., and Métoz, F. (1999). ESPript: analysis of multiple sequence alignments in PostScript. Bioinformatics *15*, 305–308.

Goujon, M., McWilliam, H., Li, W., Valentin, F., Squizzato, S., Paern, J., and Lopez, R. (2010). A new bioinformatics analysis tools framework at EMBL-EBI. Nucleic Acids Res. *38*(Web Server issue), W695–W699.

Han, K. (1996). An efficient DDAB-mediated transfection of *Drosophila* S2 cells. Nucleic Acids Res. *24*, 4362–4363.

Hansen, J.D., Du Pasquier, L., Lefranc, M.-P., Lopez, V., Benmansour, A., and Boudinot, P. (2009). The B7 family of immunoregulatory receptors: a comparative and evolutionary perspective. Mol. Immunol. *46*, 457–472.

Hashiguchi, M., Kobori, H., Ritprajak, P., Kamimura, Y., Kozono, H., and Azuma, M. (2008). Triggering receptor expressed on myeloid cell-like transcript 2 (TLT-2) is a counter-receptor for B7-H3 and enhances T cell responses. Proc. Natl. Acad. Sci. USA *105*, 10495–10500.

Hatherley, D., Graham, S.C., Turner, J., Harlos, K., Stuart, D.I., and Barclay, A.N. (2008). Paired receptor specificity explained by structures of signal regulatory proteins alone and complexed with CD47. Mol. Cell *31*, 266–277.

Kobori, H., Hashiguchi, M., Piao, J., Kato, M., Ritprajak, P., and Azuma, M. (2010). Enhancement of effector CD8+ T-cell function by tumour-associated B7-H3 and modulation of its counter-receptor triggering receptor expressed on myeloid cell-like transcript 2 at tumour sites. Immunology *130*, 363–373.

Larkin, M.A., Blackshields, G., Brown, N.P., Chenna, R., McGettigan, P.A., McWilliam, H., Valentin, F., Wallace, I.M., Wilm, A., Lopez, R., et al. (2007). Clustal W and Clustal X version 2.0. Bioinformatics *23*, 2947–2948.

Lázár-Molnár, E., Yan, Q., Cao, E., Ramagopal, U., Nathenson, S.G., and Almo, S.C. (2008). Crystal structure of the complex between programmed death-1 (PD-1) and its ligand PD-L2. Proc. Natl. Acad. Sci. USA *105*, 10483–10488.

Leitner, J., Klauser, C., Pickl, W.F., Stöckl, J., Majdic, O., Bardet, A.F., Kreil, D.P., Dong, C., Yamazaki, T., Zlabinger, G., et al. (2009). B7-H3 is a potent inhibitor of human T-cell activation: no evidence for B7-H3 and TREML2 interaction. Eur. J. Immunol. *39*, 1754–1764.

Lin, D.Y., Tanaka, Y., Iwasaki, M., Gittis, A.G., Su, H.P., Mikami, B., Okazaki, T., Honjo, T., Minato, N., and Garboczi, D.N. (2008). The PD-1/PD-L1 complex resembles the antigen-binding Fv domains of antibodies and T cell receptors. Proc. Natl. Acad. Sci. USA *105*, 3011–3016.

Ling, V., Wu, P.W., Spaulding, V., Kieleczawa, J., Luxenberg, D., Carreno, B.M., and Collins, M. (2003). Duplication of primate and rodent B7-H3 immunoglobulin V- and C-like domains: divergent history of functional redundancy and exon loss. Genomics *82*, 365–377.

Long, F., Vagin, A.A., Young, P., and Murshudov, G.N. (2008). BALBES: a molecular-replacement pipeline. Acta Crystallogr. D Biol. Crystallogr. *64*, 125–132.

Loos, M., Hedderich, D.M., Friess, H., and Kleeff, J. (2010). B7-h3 and its role in antitumor immunity. Clin. Dev. Immunol. *2010*, 683875.

Murshudov, G.N., Vagin, A.A., and Dodson, E.J. (1997). Refinement of macromolecular structures by the maximum-likelihood method. Acta Crystallogr. D Biol. Crystallogr. *53*, 240–255.

Prasad, D.V.R., Nguyen, T., Li, Z., Yang, Y., Duong, J., Wang, Y., and Dong, C. (2004). Murine B7-H3 is a negative regulator of T cells. J. Immunol. *173*, 2500–2506.

Roth, T.J., Sheinin, Y., Lohse, C.M., Kuntz, S.M., Frigola, X., Inman, B.A., Krambeck, A.E., McKenney, M.E., Karnes, R.J., Blute, M.L., et al. (2007). B7-H3 ligand expression by prostate cancer: a novel marker of prognosis and potential target for therapy. Cancer Res. *67*, 7893–7900.

Schwartz, J.C., Zhang, X., Fedorov, A.A., Nathenson, S.G., and Almo, S.C. (2001). Structural basis for co-stimulation by the human CTLA-4/B7-2 complex. Nature *410*, 604–608.

Sharpe, A.H., and Freeman, G.J. (2002). The B7-CD28 superfamily. Nat. Rev. Immunol. *2*, 116–126.

Sonnen, A.F., Yu, C., Evans, E.J., Stuart, D.I., Davis, S.J., and Gilbert, R.J. (2010). Domain metastability: a molecular basis for immunoglobulin deposition? J. Mol. Biol. *399*, 207–213.

Spinelli, S., Desmyter, A., Frenken, L., Verrips, T., Tegoni, M., and Cambillau, C. (2004). Domain swapping of a llama VHH domain builds a crystal-wide beta-sheet structure. FEBS Lett. *564*, 35–40.

Stamper, C.C., Zhang, Y., Tobin, J.F., Erbe, D.V., Ikemizu, S., Davis, S.J., Stahl, M.L., Seehra, J., Somers, W.S., and Mosyak, L. (2001). Crystal structure of the B7-1/CTLA-4 complex that inhibits human immune responses. Nature *410*, 608–611.

Steinberger, P., Majdic, O., Derdak, S.V., Pfistershammer, K., Kirchberger, S., Klauser, C., Zlabinger, G., Pickl, W.F., Stöckl, J., and Knapp, W. (2004). Molecular characterization of human 4Ig-B7-H3, a member of the B7 family with four Ig-like domains. J. Immunol. *172*, 2352–2359.

Suh, W.K., Gajewska, B.U., Okada, H., Gronski, M.A., Bertram, E.M., Dawicki, W., Duncan, G.S., Bukczynski, J., Plyte, S., Elia, A., et al. (2003). The B7 family member B7-H3 preferentially down-regulates T helper type 1-mediated immune responses. Nat. Immunol. *4*, 899–906.

Sun, P.D., and Boyington, J.C. (2001). Overview of protein folds in the immune system. Curr. Protoc. Immunol. *Appendix 1*, Appendix 1N.

Sun, M., Richards, S., Prasad, D.V.R., Mai, X.M., Rudensky, A., and Dong, C. (2002). Characterization of mouse and human B7-H3 genes. J. Immunol. *168*, 6294–6297.

Sun, X., Vale, M., Leung, E., Kanwar, J.R., Gupta, R., and Krissansen, G.W. (2003). Mouse B7-H3 induces antitumor immunity. Gene Ther. *10*, 1728–1734.

Winn, M.D., Ballard, C.C., Cowtan, K.D., Dodson, E.J., Emsley, P., Evans, P.R., Keegan, R.M., Krissinel, E.B., Leslie, A.G., McCoy, A., et al. (2011). Overview of the CCP4 suite and current developments. Acta Crystallogr. D Biol. Crystallogr. *67*, 235–242.

Xu, J., Huang, B., Xiong, P., Feng, W., Xu, Y., Fang, M., Zheng, F., and Gong, F. (2006). Soluble mouse B7-H3 down-regulates dendritic cell stimulatory capacity to allogenic T cell proliferation and production of IL-2 and IFN-gamma. Cell. Mol. Immunol. *3*, 235–240.

Yamato, I., Sho, M., Nomi, T., Akahori, T., Shimada, K., Hotta, K., Kanehiro, H., Konishi, N., Yagita, H., and Nakajima, Y. (2009). Clinical importance of B7-H3 expression in human pancreatic cancer. Br. J. Cancer *101*, 1709–1716.

 ©2013 Elsevier Ltd All rights reserved

Yang, J., Jaramillo, A., Shi, R., Kwok, W.W., and Mohanakumar, T. (2004). In vivo biotinylation of the major histocompatibility complex (MHC) class II/peptide complex by coexpression of BirA enzyme for the generation of MHC class II/tetramers. Hum. Immunol. *65*, 692–699.

Zang, X., Thompson, R.H., Al-Ahmadie, H.A., Serio, A.M., Reuter, V.E., Eastham, J.A., Scardino, P.T., Sharma, P., and Allison, J.P. (2007). B7-H3 and B7x are highly expressed in human prostate cancer and associated with disease spread and poor outcome. Proc. Natl. Acad. Sci. USA *104*, 19458–19463.

Zang, X., Sullivan, P.S., Soslow, R.A., Waitz, R., Reuter, V.E., Wilton, A., Thaler, H.T., Arul, M., Slovin, S.F., Wei, J., et al. (2010). Tumor associated endothelial expression of B7-H3 predicts survival in ovarian carcinomas. Mod. Pathol. *23*, 1104–1112.

 ©2013 Elsevier Ltd All rights reserved

Structure, Volume *21*

Supplemental information

Structure and T Cell Inhibition Properties of B7 Family Member, B7-H3

Vladimir Vigdorovich, Udupi A. Ramagopal, Eszter Lázár-Molnár, Eliezer Sylvestre, Jun Sik Lee, Kimberly A. Hofmeyer, Xingxing Zang, Stanley G. Nathenson, and Steven C. Almo

Inventory of Supplemental Information

1) Figure S1, related to Figure 2.

Stereo version of the view shown in Figure 2B.

2) Figure S2, related to Figure 3.

T-cell proliferation data obtained for $CD4^+$ cells isolated from C57BL/6 animals which possess wild-type T-cell receptor genes, unlike the experiments using OT-II cells shown in Figure 3C.

3) Figure S3, related to Table 2.

Kinetic plot for the mB7H3 dimerization.

Supplemental Data

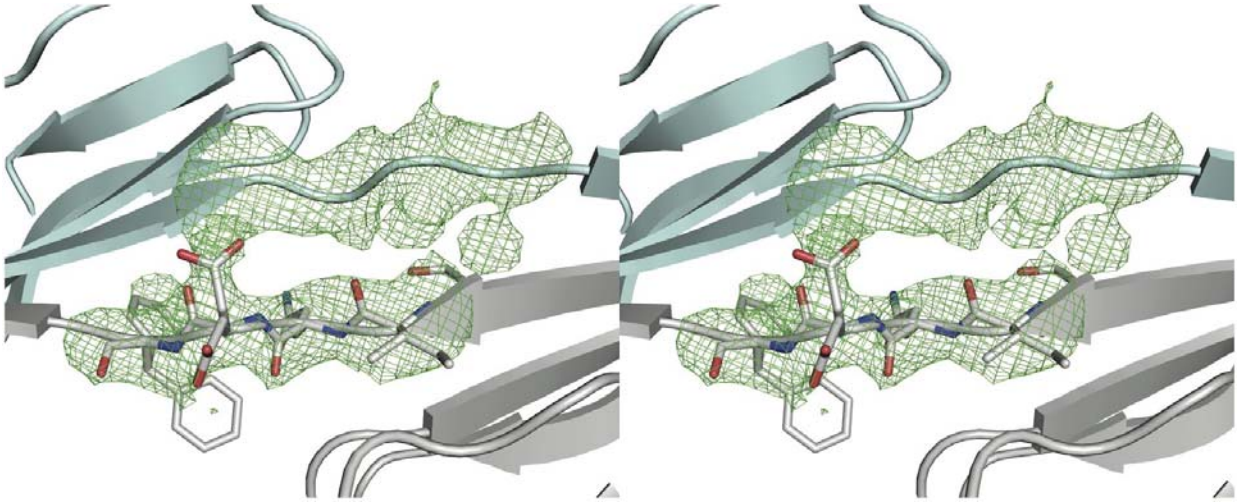


Figure S1

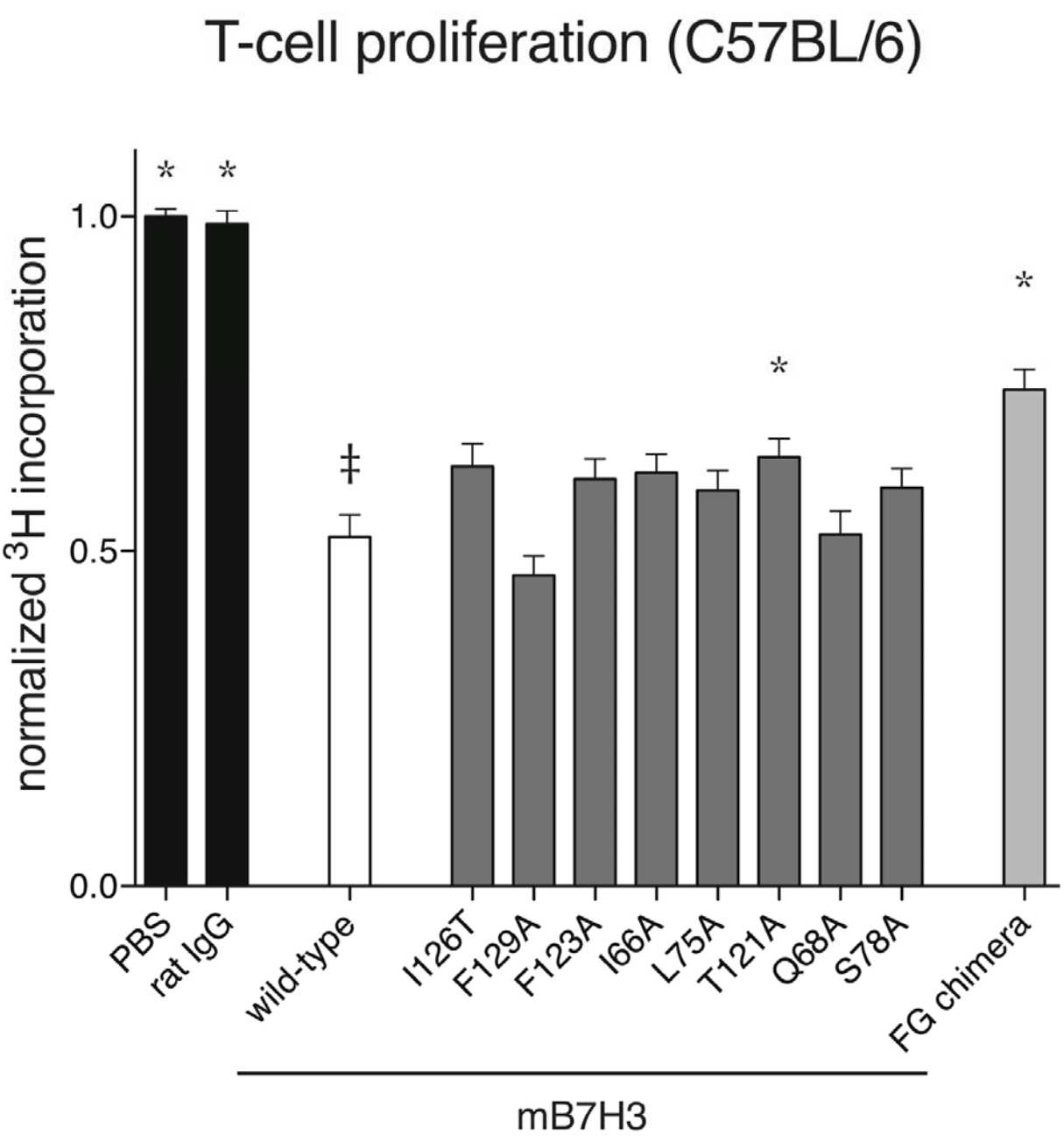

T-cell proliferation (C57BL/6)
normalized ^{3}H incorporation
1.0
0.5
0.0
*
*
‡
*
*
PBS
rat IgG
wild-type
I126T
F129A
F123A
I66A
L75A
T121A
Q68A
S78A
FG chimera
mB7H3

Figure S2

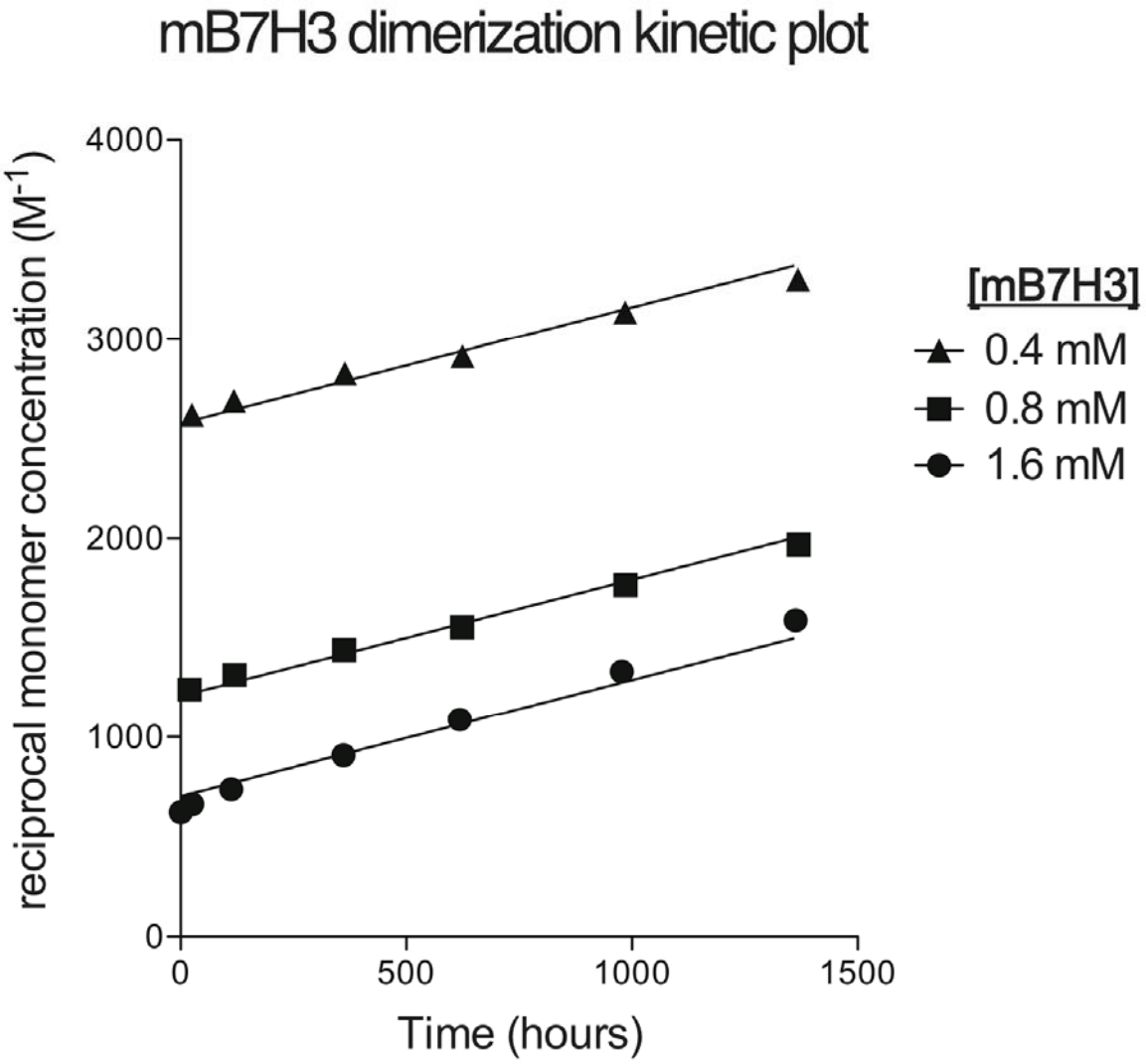

mB7H3 dimerization kinetic plot
reciprocal monomer concentration (M-1)
4000
3000
2000
1000
0
0
500
1000
1500
Time (hours)
[mB7H3]
0.4 mM
0.8 mM
1.6 mM

Figure S3

Figure S1. Stereo view of the electron density of the extended FG-loop bridging sequence. Related to Figure 2B.

Mesh representation of the *Fo–Fc* electron density map, calculated with the FG-loop sequence omitted, contoured at +3σ is shown in green near the location of the strand exchange outlined by a box in Fig. 2A. Ribbon diagrams representing the structure for each mB7H3 protomer are shown. The sidechains of the FG-loop residues are shown in gray stick-figure representation.

Figure S2. Functional characterization of wild-type and mutant mB7H3 using T cells derived from C57BL/6 mice. Related to Figure 3C.

$CD4^+$ T cells were cultured in 96-well plates precoated with 0.5 μg/mL anti-CD3 and 5 μg/mL proteins indicated along the x-axis. T-cell proliferation was assayed by pulsing with [^{3}H]-thymidine during the last 18 hours of a 3-day incubation. Data were normalized to the mean value obtained for anti-CD3 alone (PBS). Average values obtained from 5 experiments (4 replicates per sample per experiment) are shown with error bars representing the standard error of mean. Statistically significant differences ($p < 0.05$, ANOVA) with respect to the wild-type mB7H3 sample (double dagger) are labeled with asterisks.

Figure S3. Kinetic plot for the mB7H3 dimerization. Related to Figure 4 and Table 2.

Reciprocal of the concentration of mB7H3 monomer at 3 different concentration was estimated from the size-exclusion chromatography data (as shown in Fig. 4A) and plotted as a

function of time. Linear regression was used for global fitting of the slope for the 3 data sets and derivation of the estimated association rate constant (k_{on}) reported in Table 2.

Supplemental Experimental Procedures

DNA cloning

DNA encoding the predicted extracellular fragment of mB7H3 (amino acids 34–247) was amplified by PCR using primers containing BglII and AgeI restriction sites and cloned into the pMT/BiP/V5-His A (Invitrogen) or the pCGMbX vectors, which include a constitutively expressed *egfp* gene. Constructs containing mutations of single residues and contiguous spans were generated using Quickchange site-directed mutagenesis (Stratagene).

Cell Lines

Express Five SFM serum-free medium (Invitrogen) was used for routine culture and recombinant protein expression using *Drosophila* S2 cells. Schneider's *Drosophila* Medium (Invitrogen), supplemented with 10% fetal bovine serum, was used when transfecting the cells using the calcium phosphate method (Invitrogen). Alternatively, transfection was performed using the dimethyl dioctadecyl ammonium bromide (DDAB) method (Han, 1996) in Express Five SFM. Following cotransfection of the target-containing vector and the selection vector (pCoBlast or pCoPuro; mixed at a ratio of 1:20 with the target-containing vector), the cells were allowed to recover for ~48 hours before being selected with either 25 μg/mL Blasticidin S (Invitrogen) or 10 μg/mL puromycin (Fisher). To improve protein expression, drug-resistant cell populations were subcloned using a modified version of the limited dilution method (Yang et al., 2004). Briefly, parental S2 feeder cells were irradiated (20,000 rads) and co-plated with target stable cell populations at a ratio of 250,000:3 (feeder : target) per well of a 96-well plate. The target cells were allowed to form colonies over the course of 2–3 weeks while being

supplemented with fresh medium every 4–6 days. The colonies were then resuspended and replica-plated into an induction plate containing fresh medium supplemented with 1 mM copper sulfate. Following a 7-day incubation, the supernatants from the induction plate were screened by dot-blot using Penta-His antibody (Qiagen) to identify the high-expressors among the stable cell line populations.

Animals

C57BL/6 and OT-II mice were purchased from The Jackson Laboratory (Bar Harbor, ME), and maintained under pathogen-free conditions at the Albert Einstein College of Medicine. OT-II mice carry an MHC class-II-restricted chicken ovalbumin-specific TCR transgene, thus narrowing the specificity of their entire T-cell repertoire to just this antigen. Mice were used in the experiments at 6-12 weeks of age. All animal work was performed according to the guidelines set by the Institutional Animal Care and Use Committee.

Protein Expression and Purification

Cell lines were expanded in shaker-flask suspension cultures and induced with 1 mM copper sulfate. Cultures were harvested 7 days post-induction, centrifuged to remove cells and debris, supplemented with 150 mM NaCl and 0.02% sodium azide, and filtered using 0.22-µm membrane. The resulting clarified supernatants were flowed over a column containing Ni-NTA agarose (Qiagen), washed with TBS (20 mM Tris-HCl, pH 8; 300 mM NaCl; 0.02% sodium azide), TBS + 20 mM imidazole, and eluted using TBS + 200 mM imidazole. Eluted protein was

concentrated and further purified using gel filtration on Superdex-200 resin in HBS-E buffer (20 mM Hepes, pH 7; 150 mM NaCl; 1 mM EDTA).

Crystallization, Data Collection, and Modeling

Diffraction-quality crystals were grown in sitting-drop crystallization reactions containing 1 µL of protein solution (10 mg/mL in HBS-E) and 1 µL reservoir solution (0.1 M Hepes, pH 7.5 and 20% polyethylene glycol 10,000 [w/vol]). Crystals were cryo-protected in reservoir solution supplemented with 20% ethylene glycol (vol/vol) prior to flash-cooling in liquid nitrogen. X-ray diffraction data were collected at beamlines 24-ID-E (Advanced Photon Source, Argonne, IL) and X29 (National Synchrotron Light Source, Upton, NY).

Data were integrated using the iMosflm (Battye et al., 2011) software with subsequent processing using the programs within the CCP4 software package (Winn et al., 2011). An initial structure, based on the structure of human PD-L1 (PDB ID: 3BIK), was determined using the BALBES software package (Long et al., 2008). The model was further built using Coot (Emsley et al., 2010) and refined using REFMAC5 (Murshudov et al., 1997). The structure factors and the final model have been deposited into the Protein Data Bank and have been assigned the PDB ID 4I0K.

Dimerization Kinetics Measurements

Concentrated wild-type and mutant mB7H3 protein stocks were serially diluted in HBS-E buffer and incubated at 4ºC. Aliquots containing ~50 µg of protein were separated on a standardized analytical Superdex-200 sizing column and the peak heights (absorbance at 280

nm) corresponding to monomer and dimer protein species were recorded for the duration of each time course. Concentrations of monomer and dimer species were estimated based on the fraction of peak heights of each component with respect to total protein amount. These data were used to generate a global fit (using data from multiple concentrations of each protein) against a model for a second-order reaction rate law (as shown in Fig. S3) using GraphPad Prism (ver. 5) software to obtain the apparent association rate constants shown in Table 2.

T-cell Proliferation Assays

$CD4^+$ T cells were isolated from the spleens and superficial lymph nodes of 6–8 weeks old OT-II or C57BL/6 mice, using mouse CD4 Dynabeads and DETACHaBEADs (Invitrogen). 2×10^5 purified $CD4^+$ T cells were plated into each well of a 96-well cell culture plates pre-coated (for 16 hours at 4ºC) with 0.5-μg/mL solution of CD3ε antibody (BD Biosciences), also containing the indicated amounts of either wild-type mB7H3 monomer, mB7H3 dimer, mB7H3 mutants, rat IgG2b (Bio Express) as a protein control or a PBS control. [^{3}H]-thymidine (Perkin Elmer) was added for the last 18 hours of the 72-h cultures, and T-cell proliferation was measured by detecting ^{3}H-incorporation using a Wallac Microbeta 1450 Trilux liquid scintillation counter. Where indicated, data were normalized with respect to the average signal obtained with anti-CD3/PBS control. Replicates of at least four wells were used for each condition, and the experiments were repeated 2–5 times. Optimal concentrations of anti-CD3 and monomeric mB7H3—specific to our assay system—were determined by dose-response titration experiments such as the one shown in Fig. 3A. The data were analyzed using one-way ANOVA followed by Dunnett's multiple comparison test (GraphPad Prism, ver. 5), p values < 0.05 were considered significant.

Supplemental References:

Battye, T.G.G., Kontogiannis, L., Johnson, O., Powell, H.R., and Leslie, A.G.W. (2011). iMOSFLM: a new graphical interface for diffraction-image processing with MOSFLM. Acta Crystallogr. D Biol. Crystallogr. *67*, 271–281.

Emsley, P., Lohkamp, B., Scott, W.G., and Cowtan, K. (2010). Features and development of Coot. Acta Crystallogr. D Biol. Crystallogr. *66*, 486–501.

Han, K. (1996). An efficient DDAB-mediated transfection of Drosophila S2 cells. Nucleic Acids Res. *24*, 4362–4363.

Murshudov, G.N., Vagin, A.A., and Dodson, E.J. (1997). Refinement of macromolecular structures by the maximum-likelihood method. Acta Crystallogr. D Biol. Crystallogr. *53*, 240–255.

Winn, M.D., Ballard, C.C., Cowtan, K.D., Dodson, E.J., Emsley, P., Evans, P.R., Keegan, R.M., Krissinel, E.B., Leslie, A.G.W., McCoy, A., et al. (2011). Overview of the CCP4 suite and current developments. Acta Crystallogr. D Biol. Crystallogr. *67*, 235–242.

Yang, J., Jaramillo, A., Shi, R., Kwok, W.W., and Mohanakumar, T. (2004). In vivo biotinylation of the major histocompatibility complex (MHC) class II/peptide complex by coexpression of BirA enzyme for the generation of MHC class II/tetramers. Hum. Immunol. *65*, 692–699.